

Article

A Theoretical Study of Doping Evolution of Phonons in High-Temperature Cuprate Superconductors

Saheli Sarkar 

Division of Condensed Matter Physics and Materials Science, Brookhaven National Laboratory, Upton, NY 11973-5000, USA; ssarkar@bnl.gov

Abstract: Hole-doped high-temperature copper oxide-based superconductors (cuprates) exhibit complex phase diagrams where electronic orders like a charge density wave (CDW) and superconductivity (SC) appear at low temperatures. The origins of these electronic orders are still open questions due to their complex interplay and correlated nature. These electronic orders can modify the phonons in the system, which has also been experimentally found in several cuprates as a softening in the phonon frequency at the CDW vector. Recent experiments have revealed that the softening in phonons in cuprates due to CDW shows intriguing behavior with increasing hole doping. Hole doping can also change the underlying Fermi surface. Therefore, it is an interesting question whether the doping-induced change in the Fermi surface can affect the softening of phonons, which in turn can reveal the nature of the electronic orders present in the system. In this work, we investigate this question by studying the softening of phonons in the presence of CDW and SC within a perturbative approach developed in an earlier work. We compare the results obtained within the working model to some experiments.

Keywords: cuprates; phonon softening; charge density wave; superconductivity; hole doping



Citation: Sarkar, S. A Theoretical Study of Doping Evolution of Phonons in High-Temperature Cuprate Superconductors. *Condens. Matter* **2024**, *9*, 13. <https://doi.org/10.3390/condmat9010013>

Academic Editors: Antonio Bianconi and Yasutomo Uemura

Received: 28 November 2023

Revised: 20 December 2023

Accepted: 16 January 2024

Published: 6 February 2024



Copyright: © 2024 by the author. Licensee MDPI, Basel, Switzerland. This article is an open access article distributed under the terms and conditions of the Creative Commons Attribution (CC BY) license (<https://creativecommons.org/licenses/by/4.0/>).

1. Introduction

High-temperature copper oxide-based superconductors (cuprates) are paradigmatic examples of a complex interplay between several orders like a quasi-two-dimensional incommensurate charge density wave (CDW) [1,2] and superconductivity (SC) [3], especially in the under-doped regime of hole-doped cuprates [4]. Besides these orders, in the under-doped regime, there exist a ‘pseudogap’ phase [5–7] and a variety of other complex orders [8–11]. In addition to the observation of the CDW order in the under-doped regime, recent X-ray scattering experiments have observed CDW in over-doped samples of LSCO [12,13], even going well beyond the pseudogap region [14], and in over-doped BSCCO [15]. Furthermore, recent resonant X-ray scattering experiments have observed charge density modulations with correlation length much shorter compared to the CDW which are generally known as charge density fluctuations (CDFs) [16]. These CDFs have a dynamical nature due to finite energy and are present in an extremely large doping window starting from a highly under-doped regime and going to a highly over-doped regime [16,17]. Additionally, these dynamical CDFs persist up to a very high temperature, above the onset of CDW and even above the pseudogap temperature T_{PG} .

A change in doping not only tunes the electronic orders, but also changes the electronic structure and the associated Fermi surface. Angle-resolved photoemission spectroscopy (ARPES) experiments [18–20] measured the evolution of the Fermi surface of $\text{La}_{2-x}\text{Sr}_x\text{CuO}_4$ (LSCO) for a broad range of hole doping starting from the under-doped regime and going to the over-doped regime. Another ARPES experiment [21] measured the hole doping evolution of the Fermi surface of $\text{Bi}_2\text{Sr}_2\text{CaCu}_2\text{O}_{8+\delta}$ (BSCCO). For both the cases of LSCO and BSCCO, it is observed that the geometry of the Fermi surface changes from an open ‘hole-like’ to a closed ‘electron-like’ geometry. This type of topological transition of the Fermi surface is known as the Lifshitz transition.

Owing to such a complex phase diagram and Fermi surface evolution, the nature of the interactions which induce the electronic orders still remains an open question. A possible direction for disentangling various interactions is to study the collective modes associated with the electronic orders [22]. It is well known that CDW can couple to the phonons and in metallic systems give rise to the softening of the phonon frequency (we refer to it as phonon softening) at the wave vector associated with the CDW (Q) and below the CDW transition temperature. This is known as the ‘Kohn anomaly’ [23,24]. Interestingly, experiments have found signatures of phonon softening around Q but below the superconducting critical temperature (T_c) in several under-doped cuprates like $\text{YBa}_2\text{Cu}_3\text{O}_{7-x}$ (YBCO), $\text{Bi}_2\text{Sr}_2\text{CaCu}_2\text{O}_{8+\delta}$, $\text{La}_{2-x}\text{Ba}_x\text{CuO}_4$ (LBCO) and $\text{La}_{2-x}\text{Sr}_x\text{CuO}_4$ [25–29]. In under-doped La-based 214 compounds [29] and BSCCO [26,30], however, the phonon softening does not completely vanish at T_c . Besides the temperature evolution, the phonon softening in different cuprates also exhibits distinct features with a change in doping. Resonant inelastic X-ray scattering (RIXS) and neutron scattering experiments investigated phonons for different doping levels in $\text{Bi}_2\text{Sr}_2\text{CaCu}_2\text{O}_{8+\delta}$ [31], $\text{La}_{2-x}\text{Sr}_x\text{CuO}_4$ [29] and La-based 214 compounds [27], respectively. Remarkably, for doped BSCCO, the RIXS experiment [31] found a gradual suppression of phonon softening with an increase in doping in a broad window of an under-doping to an over-doping regime. In contrast to BSCCO, however, in doped LSCO [29], it was found that phonon softening related to charge density modulations remained unchanged in a broad window of hole doping despite a continuous change in the Fermi surface [18], before vanishing discontinuously at a critical doping.

To explain the phonon softening below T_c , in an earlier work [32], we investigated collective modes of phonons when they couple to both CDW and SC orders within a perturbative approach. We showed, for prototypical under-doped cuprates’ band structure, that a complex interplay between the CDW and SC orders and their fluctuations [33] can capture the temperature evolution of the phonon softening, especially the anomalous phonon softening below T_c . However, the evolution of the phonon softening with a change in doping was not addressed. It is especially interesting to see if the change in the Fermi surface due to doping can be captured through collective phonon modes, which can also elucidate the nature of the electronic orders present in the system.

Motivated by these, in this work we study, within our theoretical model developed in [32], the evolution of phonon softening for cuprates with a change in the geometry of the Fermi surface. In particular, we focus on two model cuprate bands replicating doped LSCO and BSCCO whose Fermi surfaces pass through a topological Lifshitz transition, where a hole-like Fermi surface transforms to an electron-like Fermi surface. We study the fate of the phonon softening approaching this transition for both of the model cuprate bands.

We organize this paper in the following manner. In Section 2, we briefly discuss the theoretical model, where the effects of CDW and SC orders on phonons are investigated. In Section 3, we study the doping evolution of the phonon softening for model Fermi surfaces representing doped LSCO and BSCCO systems. In Section 4, we present a discussion of our work and compare with experimental observations. In Section 5, we present a summary of the work.

2. Theoretical Model

In this section, we describe the theoretical model of a coupled electron–phonon system in the presence of the CDW and SC orders. The total Hamiltonian [32] is given by $H_{tot} = H_e + H_{ph} + H_{e-ph}$, with

$$\begin{aligned}
 H_e &= \sum_{k,\sigma} \tilde{\xi}_k c_{k,\sigma}^\dagger c_{k,\sigma} + \sum_{k,\sigma} (\chi_k c_{k+Q,\sigma}^\dagger c_{k,\sigma} + h.c.) + \sum_k (\Delta_k c_{k,\uparrow}^\dagger c_{-k,\downarrow}^\dagger + h.c.), \\
 H_{ph} &= \sum_q \omega_q b_q^\dagger b_q, \\
 H_{e-ph} &= (1/\sqrt{N}) \sum_q \sum_{k,\sigma} g(\mathbf{k}, \mathbf{q}) c_{k+q,\sigma}^\dagger c_{k,\sigma} (b_{-q}^\dagger + b_q).
 \end{aligned}
 \tag{1}$$

In Equation (1), H_e depicts the electronic Hamiltonian in the presence of CDW and SC orders at the mean-field level, where c_k and c_k^\dagger are the electronic annihilation and creation operators. ξ_k , χ_k and Δ_k are the tight-binding single-particle dispersion, CDW gap and SC gap, respectively. The Hamiltonian for the phonons is given by H_{ph} , where b_q and b_q^\dagger are the phonon annihilation and creation operators and ω_q is the bare phonon frequency. The interaction between electrons and phonons is given by the Hamiltonian H_{e-ph} , where $g(\mathbf{k}, \mathbf{q})$ is the electron–phonon (e-ph) coupling element and N is the number of lattice sites. In our model, we consider $g(\mathbf{k}, \mathbf{q}) = g$ a constant number. We construct the matrix H_e in the extended Nambu basis $\Psi_k^\dagger = (c_{k,\uparrow}^\dagger, c_{-k,\downarrow}, c_{k+Q,\uparrow}^\dagger, c_{-k-Q,\downarrow})$, where Q is the CDW wave vector. The Green’s function corresponding to H_e is given by $\hat{G}^{-1}(i\omega_n, \mathbf{k}) = (i\omega_n - \hat{H}_e)$ and has a matrix form as follows:

$$G^{-1} = \begin{pmatrix} i\omega_n - \xi_k & -\Delta_k & -\chi_k & 0 \\ -\Delta_k^* & i\omega_n + \xi_k & 0 & \chi_k \\ -\chi_k^* & 0 & i\omega_n - \xi_{k+Q} & -\Delta_{k+Q} \\ 0 & \chi_k^* & -\Delta_{k+Q}^* & i\omega_n + \xi_{k+Q} \end{pmatrix}, \tag{2}$$

where ω_n is the Matsubara frequency.

Now, we analyze the change in the phonon spectrum due to the presence of both CDW and superconducting order. Because of the presence of the CDW with wave vector Q , the new phonon propagator can be written in terms of a matrix Green’s function given by $D_{m,n}(\mathbf{q}, \tau) = -\langle \mathcal{T} \phi_{q+mQ}(\tau) \phi_{q+nQ}^\dagger(0) \rangle$ [34], where \mathcal{T} is the time-ordering operator and ϕ_q is given by $b_q^\dagger + b_{-q}$ with $m, n = \pm$. We also note that $D_{++} = D_{--} := D_1(z, \mathbf{q})$ and $D_{+-} = D_{-+} := D_2(z, \mathbf{q})$. The modified propagators can be calculated by treating the electron–phonon interaction perturbatively, as long as g is small. For a single-dispersionless phonon mode, an estimate for g can be obtained by using the dimensionless coupling constant $\lambda \sim \frac{g^2 N(E_F)}{v_0}$, where $N(E_F)$ is the density of states at the Fermi energy and v_0 is the bare phonon frequency. As typically $\frac{v_0}{N(E_F)} \ll 1$, the approximation remains valid even for large values of λ . Following the results obtained in the paper [32], the self-energy corrections $[\Sigma_{1,2,3,4}(z, \mathbf{q})]$ for phonon propagators due to the presence of both CDW and SC orders are

$$\begin{aligned} \Sigma_1(\omega, \mathbf{q}) &= \frac{g^2}{N} \sum_{\mathbf{k}, i\omega_n} [G_{11}(\mathbf{k}, i\omega_n) G_{33}(\mathbf{k} + \mathbf{q}, i\omega_n + i\epsilon_n) + (\mathbf{k} \rightarrow \mathbf{k} - \mathbf{q})] \\ \Sigma_2(\omega, \mathbf{q}) &= \frac{g^2}{N} \sum_{\mathbf{k}, i\omega_n} [G_{12}(\mathbf{k}, i\omega_n) G_{34}(\mathbf{k} + \mathbf{q}, i\omega_n + i\epsilon_n) + (\mathbf{k} \rightarrow \mathbf{k} - \mathbf{q})] \\ \Sigma_3(\omega, \mathbf{q}) &= \frac{g^2}{N} \sum_{\mathbf{k}, i\omega_n} [G_{13}(\mathbf{k}, i\omega_n) G_{31}(\mathbf{k} + \mathbf{q}, i\omega_n + i\epsilon_n) + (\mathbf{k} \rightarrow \mathbf{k} - \mathbf{q})] \\ \Sigma_4(\omega, \mathbf{q}) &= \frac{g^2}{N} \sum_{\mathbf{k}, i\omega_n} [G_{14}(\mathbf{k}, i\omega_n) G_{32}(\mathbf{k} + \mathbf{q}, i\omega_n + i\epsilon_n) + (\mathbf{k} \rightarrow \mathbf{k} - \mathbf{q})], \end{aligned} \tag{3}$$

where G_{ab} with $[a, b = 1, 2, 3, 4]$ are the various matrix elements of the Green’s function matrix defined in Equation (2).

The renormalized phonon propagators can be written using the Dyson equations obtained by using the above self-energies (Equation (3)). The Dyson equations are as follows [34] (also see Figure 1):

$$\begin{aligned} D_1(z, \mathbf{q}) &= D_0(z, \mathbf{q} + \mathbf{Q}) \left[1 + \Sigma_1(z, \mathbf{q}) D_1(z, \mathbf{q}) + \Sigma_2(z, \mathbf{q}) D_1(z, \mathbf{q}) \right. \\ &\quad \left. + \Sigma_3(z, \mathbf{q}) D_2(z, \mathbf{q}) + \Sigma_4(z, \mathbf{q}) D_2(z, \mathbf{q}) \right], \\ D_2(z, \mathbf{q}) &= D_0(z, \mathbf{q} - \mathbf{Q}) \left[\Sigma_1(z, \mathbf{q}) D_2(z, \mathbf{q}) + \Sigma_2(z, \mathbf{q}) D_2(z, \mathbf{q}) \right. \\ &\quad \left. + \Sigma_3(z, \mathbf{q}) D_1(z, \mathbf{q}) + \Sigma_4(z, \mathbf{q}) D_1(z, \mathbf{q}) \right], \end{aligned} \tag{4}$$

where $D_0(z, q) = 2\omega_q / (z^2 - \omega_q^2)$ is the bare phonon propagator. We obtain the renormalized modes for phonons in the presence of CDW and SC orders by decoupling Equation (4) through $D_{\pm}(z, q) = D_1(z, q) \pm D_2(z, q)$ and then solving $D_{\pm}(z, q)$ with the assumption that $\omega_{Q \pm q} \approx \omega_Q$ for small q . Finally, plugging in $D_0(z, q)$, we obtain the solutions for the renormalized phonon propagators as

$$D_{\pm}(z, q) = \frac{2\omega_Q}{z^2 - \omega_Q^2 - 2\omega_Q \Sigma_{\pm}(z, q)}, \tag{5}$$

where $\Sigma_+ = \Sigma_1 + \Sigma_2 + \Sigma_3 + \Sigma_4$ and $\Sigma_- = \Sigma_1 + \Sigma_2 - \Sigma_3 - \Sigma_4$. The dispersion of the renormalized phonon modes corresponds to the values of z for which the denominator of Equation (5) vanishes. Subsequently, keeping only q dependence in Σ , the frequency for each mode is given by

$$\Omega_{\pm}^2(q) = \omega_Q^2 + 2\omega_Q \Sigma_{\pm}(q). \tag{6}$$

We notice, that in the ordered phase where CDW and SC have formed, there are two normal phonon modes as given by Equation (6); however, we will only focus on the Ω_- mode [32]. We also notice from Equation (6) that the change in the phonon frequency of the Ω_- mode is depicted through the self-energy correction $\Sigma_-(q)$, keeping ω_Q constant. Therefore, the softening of the phonon frequency of the Ω_- mode implies a suppression in the $\Sigma_-(q)$. Hence, it is sufficient to plot the $\Sigma_-(q) \equiv \Sigma(q)$ instead of the full $\Omega(q)$, where q measures the deviation from $Q[q = 0]$.

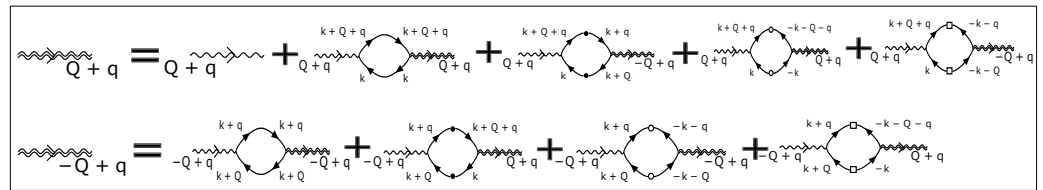


Figure 1. Diagrammatic representations of the Dyson equations for phonons in the presence of charge density wave (CDW) and superconductivity (SC). The double wavy lines represent the renormalized phonon modes. Each bubble diagram corresponds to the self-energy corrections $\Sigma_1, \Sigma_3, \Sigma_2$ and Σ_4 , respectively, and their analytic expressions are given in Equation (3).

3. Doping-Induced Fermi Surface Evolution of Phonon Softening in Cuprates

In the last section, we described the general formalism for calculating the renormalized phonon frequency in the presence of CDW and SC orders. Now, in this section, we concentrate on the specific case for the hole-doped cuprates. After decades of research on the phenomenology of the CDW phase, its correlations with superconductivity and pseudo-gap phase are strongly debated, and there is a common belief from theoretical [35,36] and experimental [37,38] studies that the CDW wave vector is incommensurate and supports a momentum space structure where the Fermi surface plays crucial roles in defining the CDW wave vector Q . Within this picture [35,36], the CDW wave vector Q is measured by connecting the ‘hot-spots’ (k -points where the Antiferromagnetic Brillouin zone boundary intersects the Fermi surface) on the Fermi surface, as indicated in Figures 2a and 3a by green arrows. In this work, we consider CDW wave vector Q , connecting the hot-spots and also considering them to be bi-axial, following our previous work [32] for our model cuprate systems. Next, following the self-consistent results of [39,40], we consider that the CDW gap χ_k is maximum (χ_{max}) near the hot-spots and falls off exponentially away from the hot-spots. The SC gap is chosen such that Δ_k gaps out the rest of the Fermi surface; however, it vanishes along the nodal direction (π, π) of the Fermi surface dictated by a d-wave symmetric SC gap, given by $\Delta_k = (\Delta_{max}/2)[\cos(k_x) - \cos(k_y)]$ [41]. Below, we separately consider Fermi surfaces’ evolutions of phonon frequencies for two tight-binding band structures which mimic $\text{Bi}_2\text{Sr}_2\text{CaCu}_2\text{O}_{8+\delta}$ (BSCCO) and $\text{La}_{2-x}\text{Sr}_x\text{CuO}_4$ (LSCO) systems.

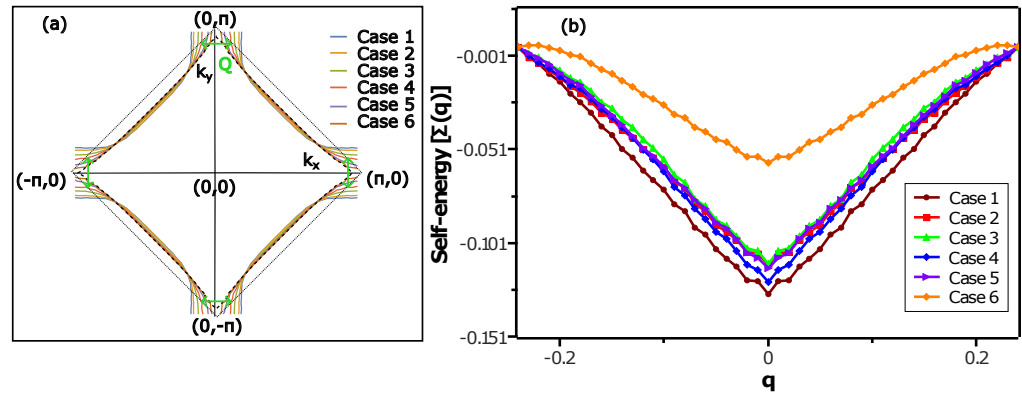


Figure 2. (a) Fermi surfaces obtained from band structure Equation (7) with different tight-binding parameters as given in Table 1. The Fermi surface evolves from hole-like to electron-like with change in the parameters. The electron-like Fermi surface is plotted with black dashed line. The tight-binding parameters corresponding to the black dashed line are given in the main text. The CDW wave vector (Q) is indicated with the green arrow. (b) Phonon softening: plots for the evolution of the self-energy $\Sigma(q)$ as a function of q for the same sets of the tight-binding parameters used in (a) and given in Table 1.

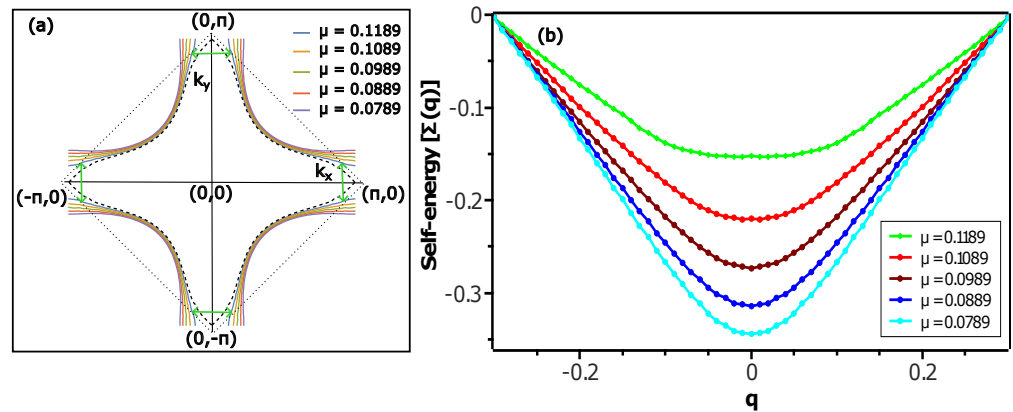


Figure 3. (a) Tight-binding Fermi surfaces obtained from Equation (8) for different values of μ . A continuous evolution from hole-like to electron-like Fermi surface can be seen with increase in μ . Electron-like Fermi surface is shown in black dashed line for $\mu = 0.1329$. The CDW wave vector (Q) is indicated with the green arrow. (b) Phonon softening: plots of the self-energy $\Sigma(q)$ of phonons as a function of q and for the same values of μ used in (a).

Table 1. Table for tight-binding parameters (in eV units) used in Equation (7) and resulting in the six Fermi surfaces, as plotted with solid lines in Figure 2a.

Tight-Binding Parameters						
Case:	t_1	t_2	t_3	t_4	t_5	μ
1	-0.7823	0.0740	-0.0587	-0.1398	-0.0174	0.0801
2	-0.7823	0.0740	-0.0487	-0.1398	-0.0074	0.080
3	-0.7823	0.0740	-0.0287	-0.1398	-0.0044	0.0795
4	-0.7823	0.0740	-0.0187	-0.1398	-0.0024	0.0793
5	-0.7823	0.0740	-0.0087	-0.1398	-0.0014	0.079
6	-0.7823	0.0740	-0.006	-0.1398	-0.00038	0.0789

3.1. Case of $La_{2-x}Sr_xCuO_4$

To capture the generic features of the Fermi surface evolution towards a topological transition in $La_{2-x}Sr_xCuO_4$, we consider a six-parameter tight-binding model band structure [42] given by

$$\begin{aligned} \tilde{\zeta}_k = & t_1 \frac{\cos(k_x) + \cos(k_y)}{2} + t_2 \cos(k_x) \cos(k_y) + t_3 \frac{\cos(2k_x) + \cos(2k_y)}{2} \\ & + t_4 \frac{(\cos(2k_x) \cos(k_y) + \cos(2k_y) \cos(k_x))}{2} + t_5 (\cos(2k_x) \cos(2k_y)) + \mu. \end{aligned} \quad (7)$$

To mimic the doping evolution of the Fermi surface on a qualitative level, we perform minimal changes in the band structure (Equation (7)) by changing only the hopping parameters t_3, t_5 and the chemical potential μ . A similar evolution of the Fermi surface is seen in the ARPES experiments [18,19] with a change in doping. The tight-binding parameters for six different cases, replicating six different Fermi surfaces considered, are given in Table 1. However, these tight-binding parameters are not fitted to the experimentally observed Fermi surfaces. The resulting Fermi surfaces for these six cases are shown in Figure 2a. We notice in Figure 2a that the Fermi surface for case 1 is hole-like featuring Fermi arcs. The geometry of the Fermi surface changes from hole-like to electron-like, going from case 1 to case 6. We depict the closed electron-like Fermi surface with a dashed black line in Figure 2a. The tight-binding parameters corresponding to the dashed black line are $t_1 = -0.7823, t_2 = 0.0740, t_3 = -0.00387, t_4 = -0.1398, t_5 = -0.00037$ and $\mu = 0.0788$. To compute the renormalized phonon frequency for the above six cases in Table 1, we choose χ_{max} and Δ_{max} to be equal to 0.1 eV, a realistic value.

The computed phonon self-energies $\Sigma(q)$ as a function of q are plotted in Figure 2b. First of all, we observe that $\Sigma(q)$ decreases strongly around $q = 0$, implying a phonon softening around Q . Also, with going away from $q = 0$, suppression in $\Sigma(q)$ is diminished, suggesting that phonon softening is reduced away from Q . Next, we closely look at the evolution of the $\Sigma(q)$ from case 1 to case 5. We observe that the strength of phonon softening remains more or less equal, as there are not many changes in $\Sigma(q)$. However, if we notice the Fermi surfaces corresponding to cases 1 to 5 in Figure 2a, we observe that the hole-like Fermi surface continuously changes towards an electronic Fermi surface. Very interestingly, we notice that for case 6, where the Fermi surface (Figure 2a) is in close vicinity to the topological Lifshitz transition, the strength of the phonon softening (Figure 2b) is significantly suppressed as compared to the earlier five cases. Hence, in the case for the model LSCO band, the strength of phonon softening changes discontinuously, remaining initially unaffected by the change in the geometry of the Fermi surface and then suddenly diminishing when the Fermi surface is very close to the Lifshitz transition.

3.2. Case of $Bi_2Sr_2CaCu_2O_{8+\delta}$

In order to capture the broad features of the evolution of the Fermi surface from hole-like to electron-like for $Bi_2Sr_2CaCu_2O_{8+\delta}$, we consider a six-parameter tight-binding model band structure [43] given by

$$\begin{aligned} \tilde{\zeta}_k = & t_1 \frac{\cos(k_x) + \cos(k_y)}{2} + t_2 \cos(k_x) \cos(k_y) + t_3 \frac{\cos(2k_x) + \cos(2k_y)}{2} \\ & + t_4 \frac{(\cos(2k_x) \cos(k_y) + \cos(2k_y) \cos(k_x))}{2} + t_5 (\cos(2k_x) \cos(2k_y)) + \mu, \end{aligned} \quad (8)$$

with $t_1 = -0.5908, t_2 = 0.0962, t_3 = -0.1306, t_4 = -0.0507$ and $t_5 = 0.0939$. Here, for simplicity, we only change the chemical potential μ to capture the qualitative behavior of the topological transition of the Fermi surface, as observed in the ARPES experiment [21]; thus, the model band is not expected to exactly fit the ARPES bands [21]. The tight-binding parameters for the band are in eV units. The resulting Fermi surfaces for different μ values are displayed in Figure 3a. We notice that the geometry of the Fermi surface continuously evolves from hole-like to electron-like with increasing μ continuously from 0.0789 to 0.1189. On further increasing μ , the Fermi surface goes through a topological Lifshitz transition.

The closed electron-like Fermi surface corresponding to a μ value of 0.1329 is plotted with a dashed black line in Figure 3a.

To study the renormalized phonon frequency, we choose both Δ_{max} and χ_{max} to be 0.02 eV, a value realistically obtained. In Figure 3b, we plot the self-energy $\Sigma(q)$ as a function of q for each of the μ values in Figure 3a. We notice that for a μ value of 0.0789, the value of the $\Sigma(q)$ is suppressed around $q = 0$, and the suppression is strongest at $q = 0$, that is, at the CDW wave vector. This implies that there is a phonon softening around the CDW wave vector. Once we go away from $q = 0$, the phonon softening is significantly reduced as the suppression in $\Sigma(q)$ is diminished. Next, we see that with an increase in the value of μ , the phonon softening becomes diminished continuously as the suppression in $\Sigma(q)$ around $q = 0$ becomes smaller with an increase in μ values. This implies that for the case of the model BSCCO band, the phonon softening continuously diminishes as the hole-like Fermi surface evolves continuously towards the topological Lifshitz transition. This continuous evolution is in stark contrast to the case for the model LSCO band, where the phonon softening changes discontinuously as the hole-like Fermi surface evolves towards the topological transition.

4. Discussion

In this work, applying a perturbative approach, we study the Fermi surface evolution of the phonon softening in model cuprate bands, specially focusing on the parameter regimes where the Fermi surface approaches a topological Lifshitz transition. In particular, we focus on two cuprate systems LSCO and BSCCO, where ARPES experiments also observed a topological transition from a hole-like Fermi surface to an electron-like Fermi surface due to a change in doping.

In this work, to only focus on the possible effects of the change in the geometry of the Fermi surface due to doping on phonon softening, we have excluded the doping dependencies of the CDW and SC gaps. Furthermore, as the theoretical tight-binding parameters are not fitted to experimental Fermi surfaces, the doping levels (x) (as shown in Figure 4a,b) and number of holes ($p = 1 + x$) per Cu atom associated with the parameters chosen in this work might differ from the experimental doping values where phonon softening occurs.

For the case of the model system representing BSCCO, we have found that the phonon softening is continuously suppressed (Figure 3b) with the continuous evolution of the Fermi surface from a hole-like to an electron-like geometry, and it is significantly suppressed close to the topological transition. For the model system of LSCO, we have found two features in the evolution of the phonon softening. First, the phonon softening remains initially unaffected, even when the Fermi surface continuously changes from a hole-like towards an electron-like geometry, which is in sharp contrast to the case of BSCCO. Second, only close to the topological transition of the Fermi surface, the phonon softening becomes significantly suppressed. This difference in the nature of evolution of the phonon softening between these two materials can be mainly attributed to the difference in the band structure and associated differences in the nesting properties of the Fermi surfaces in these systems.

It would also be interesting to compare the results obtained from the theoretical models to the experiments. However, these comparisons must be considered at a qualitative level. A recent RIXS experiment [31] measured phonon softening in BSCCO with a change in doping at T_c and below T_c . They found a gradual suppression of the phonon softening with an increase in doping from an under-doped to an over-doped regime at T_c . At a low temperature, the experiment again found a gradual suppression of phonon softening with an increase in doping in a broad window between the under-doped and over-doped regime, with one exception in the highly under-doped regime. From the calculations performed in this work for BSCCO bands, we have found a gradual suppression of phonon softening with an increase in doping, which is in general agreement to the above experimental findings. Noticeably, we have not found any enhancement of phonon softening in the under-doped regime within the parameter regime explored in this work. Therefore, it would be interesting

to investigate whether incorporating a more accurate description of the band and doping dependence of the CDW and the SC orders and also the effects of CDFs can result in such an enhancement, as seen in the extreme under-doped case in the experiment.

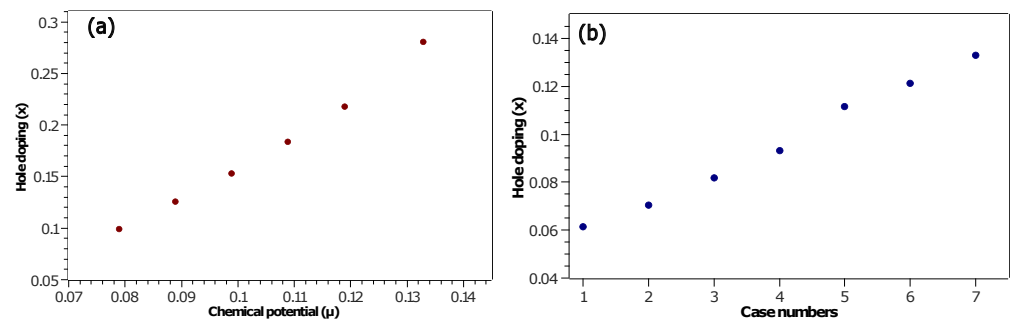


Figure 4. (a) Plot of the hole doping (x) versus chemical potential (μ) for the model tight-binding band in Equation (8) imitating BSCCO. The last point represents the doping around the topological Lifshitz transition in the theoretical model. (b) Plot of the hole doping (x) versus tight-binding parameters (shown in Table 1) for the model band in Equation (7) imitating LSCO. The last point represents the doping around the topological Lifshitz transition in the theoretical model.

Another recent RIXS experiment [29] measured the evolution of the phonon softening in LSCO in a broad doping regime across the topological Lifshitz transition. The experimental results suggest that the strength of the phonon softening associated with the CDW remains almost the same with a gradual increase in the doping, even in the vicinity of the Lifshitz transition, but it abruptly vanishes at a critical doping, where eventually the CDW order disappears. By taking into account a theoretical model of a tight-binding band for LSCO and coupling between phonons with bi-axial CDW and SC, we have found that the strength of phonon softening remains approximately the same while the Fermi surface evolves continuously towards the Lifshitz transition. This bears a resemblance to the experimental observations. Moreover, we have also found that close to the topological Lifshitz transition, the phonon softening is abruptly suppressed. This feature is in contrast to the experimental observations.

In the context of LSCO, we now discuss some aspects which need further investigation. The RIXS experiment [29] in LSCO suggests a CDW-driven phonon softening, implying that in the doping regime considered in the experiment, there might be no signature of the magnetic order and only CDW correlations survive, which is also in accordance with previous experimental observations [12,13]. Hence, our theoretical model which involves coupling between phonons, CDW and SC is a consistent model for describing phonon softening in the vicinity of the topological transition in this material. However, the effects of uni-axial stripy CDW [8,44] pertinent to LSCO, which are not currently considered in our work, can play crucial roles in describing the differences. Additionally, more accurate descriptions of the doping dependence of bands and the CDW and the SC orders can play unique roles. It should also be noted that while for LSCO, the experimental [29] wave vector corresponding to the strongest phonon softening slightly differs from the CDW wave vector (Q), within our theoretical framework, the strongest phonon softening always occurs at the CDW wave vector Q . This can be related to the fact that for simplicity we have considered in our model an electron–phonon coupling constant which is independent of both fermion and phonon momenta, while for the breathing modes in cuprates, the electron–phonon coupling can in general depend on the momenta [45] and can result in such an offset of the wave vector.

Besides the doping dependence, another vital aspect of phonon softening in cuprates is their temperature evolution. The RIXS experiment in BSCCO [31] observed an enhancement in the phonon softening between T_c and low temperature for some doping regime. The RIXS experiment [29] in LSCO measured phonon softening at T_c and above T_c . Curiously, for both BSCCO [26] and LSCO [29], the phonon softening still survives above T_c . To theoretically account for these behaviors at T_c and above, one needs to include the effects

of thermal fluctuations, the short-range nature of the CDW and also the possible coupling between CDWs and the lattice, which all can play important roles. In an earlier work [32], it was indeed found that fluctuation-driven damping effects and the interplay between the temperature dependence of CDW, SC and the damping can capture some crucial aspects of the temperature evolution of the phonon softening in the under-doped cuprates. As in this work, we work at the mean-field level, and the effects of higher temperatures cannot be properly accounted for and can also be partially responsible for the differences. Therefore, it will be an interesting future direction to theoretically study the combined temperature and doping evolution of the phonon softening in both BSCCO and LSCO.

5. Conclusions

To summarize, in this work, by employing a perturbative technique, we have theoretically studied the effect of Fermi surface evolution close to the topological Lifshitz transition on phonon softening for two simple model tight-binding band structures broadly capturing doped LSCO and doped BSCCO systems in the presence of a charge density wave and superconductivity. We have found interesting features of phonon softening in these two materials and have compared them with experimental observations.

Funding: This research was funded by the Office of Basic Energy Sciences, Material Sciences and Engineering Division, U. S. Department of Energy, under Contract No. DE-SC0012704.

Data Availability Statement: The raw data supporting the conclusions of this article will be made available by the authors on request.

Conflicts of Interest: The author declares no conflicts of interest.

Abbreviations

The following abbreviations are used in this manuscript:

CDW	charge density wave
SC	superconductivity
BSCCO	$\text{Bi}_2\text{Sr}_2\text{CaCu}_2\text{O}_{8+\delta}$
LSCO	$\text{La}_{2-x}\text{Sr}_x\text{CuO}_4$
YBCO	$\text{YBa}_2\text{Cu}_3\text{O}_{7-x}$
LBCO	$\text{La}_{2-x}\text{Ba}_x\text{CuO}_4$
ARPES	angle-resolved photoemission spectroscopy
RIXS	resonant inelastic X-ray scattering

References

- Hoffman, J.E.; Hudson, E.W.; Lang, K.M.; Madhavan, V.; Eisaki, H.; Uchida, S.I.; Davis, J.C. A four unit cell periodic pattern of quasi-particle states surrounding vortex cores in $\text{Bi}_2\text{Sr}_2\text{CaCu}_2\text{O}_{8+\delta}$. *Science* **2002**, *295*, 466–469. [[CrossRef](#)] [[PubMed](#)]
- Ghiringhelli, G.; Le Tacon, M.; Minola, M.; Blanco-Canosa, S.; Mazzoli, C.; Brookes, N.B.; De Luca, G.M.; Frano, A.; Hawthorn, D.G.; He, F.; et al. Long-range incommensurate charge fluctuations in (Y, Nd) $\text{Ba}_2\text{Cu}_3\text{O}_{6+x}$. *Science* **2012**, *337*, 821–825. [[CrossRef](#)] [[PubMed](#)]
- Tsuei, C.C.; Kirtley, J.R. Pairing symmetry in cuprate superconductors. *Rev. Mod. Phys.* **2000**, *72*, 969. [[CrossRef](#)]
- Fradkin, E.; Kivelson, S.A.; Tranquada, J.M. Colloquium: Theory of intertwined orders in high temperature superconductors. *Rev. Mod. Phys.* **2015**, *87*, 457. [[CrossRef](#)]
- Alloul, H.; Ohno, T.; Mendels, P. 89Y NMR Evidence for a Fermi-Liquid Behavior in $\text{YBa}_2\text{Cu}_3\text{O}_{6+x}$. *Phys. Rev. Lett.* **1989**, *63*, 1700. [[CrossRef](#)]
- Renner, C.; Revaz, B.; Genoud, J.-Y.; Kadowaki, K.; Fischer, O. Pseudogap Precursor of the Superconducting Gap in Under and Overdoped $\text{Bi}_2\text{Sr}_2\text{CaCu}_2\text{O}_{8+\delta}$. *Phys. Rev. Lett.* **1998**, *80*, 149. [[CrossRef](#)]
- Ino, A.; Mizokawa, T.; Kobayashi, K.; Fujimori, A.; Sasagawa, T.; Kimura, T.; Kishio, K.; Tamasaku, K.; Eisaki, H.; Uchida, S. Doping Dependent Density of States and Pseudogap Behavior in $\text{La}_{2-x}\text{Sr}_x\text{CuO}_4$. *Phys. Rev. Lett.* **1998**, *81*, 2124. [[CrossRef](#)]
- Emery, V.J.; Kivelson, S.A.; Tranquada, J.M. Stripe phases in high-temperature superconductors. *Proc. Natl. Acad. Sci. USA* **1999**, *96*, 8814–8817. [[CrossRef](#)]
- Fauque, B.; Sidis, Y.; Hinkov, V.; Pailhes, S.; Lin, C.T.; Chaud, X.; Bourges, P. Magnetic order in the pseudogap phase of high- T_c superconductors. *Phys. Rev. Lett.* **2006**, *96*, 197001. [[CrossRef](#)]
- Sarkar, S.; Chakraborty, D.; Pepin, C. Incipient loop-current order in the underdoped cuprate superconductors. *Phys. Rev. B* **2019**, *100*, 214519. [[CrossRef](#)]

11. He, R.H.; Hashimoto, M.; Karapetyan, H.; Koralek, J.D.; Hinton, J.P.; Testaud, J.P.; Nathan, V.; Yoshida, Y.; Yao, H.; Tanaka, K.; et al. From a single-band metal to a high-temperature superconductor via two thermal phase transitions. *Science* **2011**, *331*, 1579–1583. [[CrossRef](#)] [[PubMed](#)]
12. Wen, J.J.; Huang, H.; Lee, S.J.; Jang, H.; Knight, J.; Lee, Y.S.; Fujita, M.; Suzuki, K.M.; Asano, S.; Kivelson, S.A.; et al. Observation of two types of charge-density-wave orders in superconducting $\text{La}_{2-x}\text{Sr}_x\text{CuO}_4$. *Nat. Commun.* **2019**, *10*, 3269. [[CrossRef](#)] [[PubMed](#)]
13. von Arx, K.; Wang, Q.; Mustafi, S.; Mazzone, D.G.; Horio, M.; Mukkattukavil, D.J.; Pomjakushina, E.; Pyon, S.; Takayama, T.; Takagi, H.; et al. Fate of charge order in overdoped La-based cuprates. *NPJ Quantum Mater.* **2023**, *8*, 7. [[CrossRef](#)]
14. Li, Q.; Huang, H.Y.; Ren, T.; Weschke, E.; Ju, L.; Zou, C.; Zhang, S.; Qiu, Q.; Liu, J.; Ding, S.; et al. Prevailing Charge Order in Overdoped $\text{La}_{2-x}\text{Sr}_x\text{CuO}_4$ beyond the Superconducting Dome. *Phys. Rev. Lett.* **2023**, *131*, 116002. [[CrossRef](#)] [[PubMed](#)]
15. Peng, Y.Y.; Fumagalli, R.; Ding, Y.; Minola, M.; Caprara, S.; Betto, D.; Bluschke, M.; De Luca, G.M.; Kummer, K.; Lefrançois, E.; et al. Re-entrant charge order in overdoped $(\text{Bi,Pb})_{2.12}\text{Sr}_{1.88}\text{CuO}_{6+\delta}$ outside the pseudogap regime. *Nat. Mater.* **2018**, *17*, 697–702. [[CrossRef](#)] [[PubMed](#)]
16. Arpaia, R.; Martinelli, L.; Sala, M.M.; Caprara, S.; Nag, A.; Brookes, N.B.; Camisa, P.; Li, Q.; Gao, Q.; Zhou, X.; et al. Signature of quantum criticality in cuprates by charge density fluctuations. *Nat. Commun.* **2023**, *14*, 7198. [[CrossRef](#)] [[PubMed](#)]
17. Arpaia, R.; Caprara, S.; Fumagalli, R.; De Vecchi, G.; Peng, Y.Y.; Andersson, E.; Betto, D.; De Luca, G.M.; Brookes, N.B.; Lombardi, F.; et al. Dynamical charge density fluctuations pervading the phase diagram of a Cu-based high- T_c superconductor. *Science* **2019**, *365*, 906–910. [[CrossRef](#)]
18. Yoshida, T.; Zhou, X.J.; Tanaka, K.; Yang, W.L.; Hussain, Z.; Shen, Z.X.; Fujimori, A.; Sahrakorpi, S.; Lindroos, M.; Markiewicz, R.S.; et al. Systematic doping evolution of the underlying Fermi surface of $\text{La}_{2-x}\text{Sr}_x\text{CuO}_4$. *Phys. Rev. B* **2006**, *74*, 224510. [[CrossRef](#)]
19. Fujimori, A.; Ino, A.; Mizokawa, T.; Kim, C.; Shen, Z.X.; Sasagawa, T.; Kimura, T.; Kishio, K.; Takaba, M.; Tamasaku, K.; et al. Chemical potential shift, density of states and Fermi surfaces in overdoped and underdoped $\text{La}_{2-x}\text{Sr}_x\text{CuO}_4$. *J. Phys. Chem. Solids* **1998**, *59*, 1892–1896. [[CrossRef](#)]
20. Zhong, Y.; Chen, Z.; Chen, S.D.; Xu, K.J.; Hashimoto, M.; He, Y.; Uchida, S.I.; Lu, D.; Mo, S.K.; Shen, Z.X.; et al. Differentiated roles of Lifshitz transition on thermodynamics and superconductivity in $\text{La}_{2-x}\text{Sr}_x\text{CuO}_4$. *Proc. Natl. Acad. Sci. USA* **2023**, *119*, e2204630119. [[CrossRef](#)]
21. Kaminski, A.; Rosenkranz, S.; Fretwell, H.M.; Norman, M.R.; Randeria, M.; Campuzano, J.C.; Park, J.M.; Li, Z.Z.; Raffy, H. Change of Fermi-surface topology in $\text{Bi}_2\text{Sr}_2\text{CaCu}_2\text{O}_{8+\delta}$ with doping. *Phys. Rev. B* **2006**, *73*, 174511. [[CrossRef](#)]
22. Loret, B.; Auvray, N.; Gallais, Y.; Cazayous, M.; Forget, A.; Colson, D.; Julien, M.-H.; Paul, I.; Civelli, M.; Sacuto, A. Intimate link between charge density wave, pseudogap and superconducting energy scales in cuprates. *Nat. Phys.* **2019**, *15*, 771–775. [[CrossRef](#)]
23. Woll, E.J., Jr.; Kohn, W. Images of the fermi surface in phonon spectra of metals. *Phys. Rev.* **1962**, *126*, 1693. [[CrossRef](#)]
24. Renker, B.; Rietschel, H.; Pintschovius, L.; Gläser, W.; Brüesch, P.; Kuse, D.; Rice, M.J. Observation of Giant Kohn Anomaly in the One-Dimensional Conductor $\text{K}_2\text{Pt}(\text{CN})_4\text{Br}_{0.3}\cdot 3\text{H}_2\text{O}$. *Phys. Rev. Lett.* **1973**, *30*, 1144. [[CrossRef](#)]
25. Le Tacon, M.; Bosak, A.; Souliou, S.M.; Dellea, G.; Loew, T.; Heid, R.; Bohnen, K.P.; Ghiringhelli, G.; Krisch, M.; Keimer, B. Inelastic X-ray scattering in $\text{YBa}_2\text{Cu}_3\text{O}_{6.6}$ reveals giant phonon anomalies and elastic central peak due to charge-density-wave formation. *Nat. Phys.* **2014**, *10*, 52–58. [[CrossRef](#)]
26. Lee, W.S.; Zhou, K.J.; Hepting, M.; Li, J.; Nag, A.; Walters, A.C.; Garcia-Fernandez, M.; Robarts, H.C.; Hashimoto, M.; Lu, H.; et al. Spectroscopic fingerprint of charge order melting driven by quantum fluctuations in a cuprate. *Nat. Phys.* **2021**, *17*, 53–57. [[CrossRef](#)]
27. Reznik, D.; Pintschovius, L.; Ito, M.; Iikubo, S.; Sato, M.; Goka, H.; Fujita, M.; Yamada, K.; Gu, G.D.; Tranquada, J.M. Electron-phonon coupling reflecting dynamic charge inhomogeneity in copper oxide superconductors. *Nature* **2006**, *440*, 1170–1173. [[CrossRef](#)] [[PubMed](#)]
28. McQueeney, R.J.; Petrov, Y.; Egami, T.; Yethiraj, M.; Shirane, G.; Endoh, Y. Anomalous dispersion of LO phonons in $\text{La}_{1.85}\text{Sr}_{0.15}\text{CuO}_4$ at low temperatures. *Phys. Rev. Lett.* **1999**, *82*, 628. [[CrossRef](#)]
29. Lin, J.Q.; Miao, H.; Mazzone, D.G.; Gu, G.D.; Nag, A.; Walters, A.C.; García-Fernández, M.; Barbour, A.; Pellicciari, J.; Jarrige, I.; et al. Strongly correlated charge density wave in $\text{La}_{2-x}\text{Sr}_x\text{CuO}_4$ evidenced by doping-dependent phonon anomaly. *Phys. Rev. Lett.* **2020**, *124*, 207005. [[CrossRef](#)]
30. Wang, Q.; von Arx, K.; Horio, M.; Mukkattukavil, D.J.; Küspert, J.; Sassa, Y.; Schmitt, T.; Nag, A.; Pyon, S.; Takayama, T.; et al. Charge order lock-in by electron-phonon coupling in $\text{La}_{1.675}\text{Eu}_{0.2}\text{Sr}_{0.125}\text{CuO}_4$. *Sci. Adv.* **2021**, *7*, eabg7394. [[CrossRef](#)]
31. Lu, H.; Hashimoto, M.; Chen, S.D.; Ishida, S.; Song, D.; Eisaki, H.; Nag, A.; Garcia-Fernandez, M.; Arpaia, R.; Ghiringhelli, G.; et al. Identification of a characteristic doping for charge order phenomena in Bi-2212 cuprates via RIXS. *Phys. Rev. B* **2022**, *106*, 155109. [[CrossRef](#)]
32. Sarkar, S.; Grandadam, M.; Pepin, C. Anomalous softening of phonon dispersion in cuprate superconductors. *Phys. Rev. Res.* **2021**, *3*, 013162. [[CrossRef](#)]
33. Pepin, C.; Chakraborty, D.; Grandadam, M.; Sarkar, S. Fluctuations and the Higgs mechanism in underdoped cuprates. *Annu. Rev. Condens. Matter Phys.* **2020**, *11*, 301–323. [[CrossRef](#)]
34. Lee, P.A.; Rice, T.M.; Anderson, P.W. Conductivity from charge or spin density waves. *Solid State Commun.* **1993**, *88*, 1001. [[CrossRef](#)]
35. Efetov, K.B., Meier, H. and Pepin, C. Pseudogap state near a quantum critical point. *Nat. Phys.* **2013**, *9*, 442–446. [[CrossRef](#)]

36. Wang, Y.; Chubukov, A. Charge-density-wave order with momentum $(2 Q, 0)$ and $(0, 2 Q)$ within the spin-fermion model: Continuous and discrete symmetry breaking, preemptive composite order, and relation to pseudogap in hole-doped cuprates. *Phys. Rev. B* **2014**, *90*, 035149. [[CrossRef](#)]
37. da Silva Neto, E.H.; Aynajian, P.; Frano, A.; Comin, R.; Schierle, E.; Weschke, E.; Gyenis, A.; Wen, J.; Schneeloch, J.; Xu, Z.; et al. Ubiquitous interplay between charge ordering and high-temperature superconductivity in cuprates. *Science* **1993**, *343*, 393–396. [[CrossRef](#)]
38. Comin, R.; Frano, A.; Yee, M.M.; Yoshida, Y.; Eisaki, H.; Schierle, E.; Weschke, E.; Sutarto, R.; He, F.; Soumyanarayanan, A.; He, Y. Charge order driven by Fermi-arc instability in $\text{Bi}_2\text{Sr}_{2-x}\text{La}_x\text{CuO}_{6+\delta}$. *Science* **2014**, *342*, 390–392. [[CrossRef](#)] [[PubMed](#)]
39. Grandadam, M.; Chakraborty, D.; Montiel, X.; Pépin, C. Electronic spectral function in the fractionalized pair density wave scenario. *Phys. Rev. B* **2020**, *102*, 121104(R). [[CrossRef](#)]
40. Chakraborty, D.; Grandadam, M.; Hamidian, M.H.; Davis, J.C.S. Sidis, Y.; Pépin, C. Fractionalized pair density wave in the pseudogap phase of cuprate superconductors. *Phys. Rev. B* **2019**, *100*, 224511. [[CrossRef](#)]
41. Scalapino, D.J. The case for $d_{x^2-y^2}$ pairing in the cuprate superconductors. *Phys. Rep.* **1995**, *250*, 329–365. [[CrossRef](#)]
42. Chakraborty, D.; Black-Schaffer, A.M. Odd-frequency pair density wave correlations in underdoped cuprates. *New J. Phys.* **2021**, *23*, 033001. [[CrossRef](#)]
43. Eschrig, M.; Norman, M.R. Effect of the magnetic resonance on the electronic spectra of high T_c superconductors. *Phys. Rev. B* **2003**, *67*, 144503. [[CrossRef](#)]
44. Tranquada, J.M.; Sternlieb, B.J.; Axe, J.D.; Nakamura, Y.; Uchida, S.I. Evidence for stripe correlations of spins and holes in copper oxide superconductors. *Nature* **1995**, *375*, 561–563. [[CrossRef](#)]
45. Devereaux, T.P.; Cuk, T.; Shen, Z.X.; Nagaosa, N. Anisotropic electron-phonon interaction in the cuprates. *Phys. Rev. Lett.* **2004**, *93*, 117004. [[CrossRef](#)]

Disclaimer/Publisher’s Note: The statements, opinions and data contained in all publications are solely those of the individual author(s) and contributor(s) and not of MDPI and/or the editor(s). MDPI and/or the editor(s) disclaim responsibility for any injury to people or property resulting from any ideas, methods, instructions or products referred to in the content.